Composites: Part A 94 (2017) 189–198

Contents lists available at ScienceDirect

Composites: Part A

journal homepage: www.elsevier.com/locate/compositesa

Modelling of carbon nanotube dispersion and strengthening mechanisms in Al matrix composites prepared by high energy ball milling-powder metallurgy method

Z.Y. Liu [a], B.L. Xiao [a], W.G. Wang [b], Z.Y. Ma [a,*]

[a] Shenyang National Laboratory for Materials Science, Institute of Metal Research, Chinese Academy of Sciences, 72 Wenhua Road, Shenyang 110016, China
[b] Liaoning Shihua University, 1 Dandong Road, Fushun 113001, China

ARTICLE INFO

Article history:
Received 24 August 2016
Accepted 27 November 2016
Available online 22 December 2016

Keywords:
A. Metal-matrix composites (MMCs)
A. Carbon nanotube
B. Strength
C. Analytical modelling

ABSTRACT

Carbon nanotube (CNT) reinforced Al-5Mg composites were prepared by combining ball milling, hot-pressing and subsequent hot extrusion. CNT distribution during milling and strengthening mechanism of the composites were investigated. A model based on the ratio of minimum necessary time for uniformly dispersing CNT to flattening time of composite powders was proposed to analyze the effect of milling rotation rate on CNT distribution, and it indicated that both low and high milling rotation rates are not beneficial to CNT distribution, due to small deformation ratio and severe cold-welding, respectively. Under a milling rotation rate of 400 rpm, CNTs could be uniformly dispersed after 8 h of milling and aligned along the extruding direction after extrusion. Elastic moduli and strengths of the composites were significantly increased. Load transfer, grain refinement, and mismatch dislocation mechanisms were determined to contribute to the strength increase of CNT/Al-5Mg composites.

1. Introduction

The incorporating of reinforcements into structural materials is an effective way of producing stronger materials with excellent strength and stiffness [1]. As a new type of reinforcement, carbon nanotubes (CNTs) are now considered as the ideal reinforcements for composites due to their extremely high elastic modulus (~1 TPa) and strength (>30 GPa) as well as good thermal and electrical properties [2,3]. Thus, CNT reinforced metal (CNT/metal) composites have attracted great attentions in aerospace industry.

Although some novelty methods, e.g., molecular level mixing between functionalized CNTs and metal ions (Cu, Co, Ni) [4,5], and in-situ growth of CNTs on metal powders [6], have been successfully used to fabricate high-property CNT/metal composites, it is difficult to transplant these methods to industrial applications. Powder metallurgy (PM) is still the most common route for preparing CNT/metal composites. In the past few years, ball milling-PM route has been widely used to fabricate the CNT/metal composites due to its easy operation and mass production.

It was well documented that CNTs could be dispersed into metals by ball milling, thereby improving the mechanical properties of metals, especially Al [7,8]. Many researchers investigated the evolution of Al powder morphology during milling [9–11], however no relationship among mill rotation rate, powder morphology evaluation and CNT distribution has been established. As a result, choosing principle of milling conditions is still not clear for well dispersing CNTs. Furthermore, the reported studies were essentially limited to pure Al matrix. Such matrix is usually not eligible for engineering applications due to its low mechanical strength.

Strengthening mechanism is a significant guideline on composite design. The strengthening behavior of CNTs reinforced polymer composites could be well reflected by analog simulation method [12,13], however these methods are difficult to directly transport to investigate strengthening of CNT/metal composites. Some strengthening mechanisms have been reported to actually take effect in CNT/metal composites, such as load transfer and grain refinement mechanisms [2,4]. However, the other mechanisms, such as mismatch dislocation, Orowan strengthening which are commonly operative in metal matrix composites, have not been deeply discussed.

In this study, CNT/Al-5Mg composites were prepared by ball milling, hot-pressing and hot-deformation method. CNT distribution and strengthening mechanism were analyzed. The aim is (a) to establish the optimum process parameters for fabricating CNT/Al composites with uniform dispersed CNTs in milling-PM route,

* Corresponding author.
E-mail address: zyma@imr.ac.cn (Z.Y. Ma).

http://dx.doi.org/10.1016/j.compositesa.2016.11.029
1359-835X/

(b) to understand the key factors influencing the CNT distribution during milling, and (c) elucidate the strengthening mechanism of CNT/Al composites.

2. Experimental

2.1. Raw materials and composite fabrication

The matrix was Al-5wt.%Mg (Al-5Mg) alloy, a non age-hardenable Al alloy. The as-received Al-5Mg powders had an average diameter of ~10 μm (Fig. 1(a)). As-received CNTs (95–98% purity) were synthesized using chemical vapor deposition by Tsinghua University. The CNTs had entangled morphologies with a length of ~5 μm and an outer diameter of about 10 nm (Fig. 1(b)). 1.5 and 3 vol.% CNTs were ball milled with Al-5Mg alloy powders, in an attritor running at 300–450 rpm for 2–8 h with a 10:1 ball to powder ratio. Hardened steel balls with 5 mm in diameter were used. 1.5 wt.% stearic acid was added for preventing serious cold-welding.

The as-milled powders were cold-compacted in a cylinder die, degassed and hot-pressed at 753 K for 1 h, into cylindrical billets. The as-pressed billets were hot extruded at 723 K into bars with an extrusion ratio of 25:1. For comparison, an Al-5Mg alloy was also fabricated using the same routine. 3 vol.% CNT/Al-5Mg composites was annealed at 753 K for 1–4 h to identify the thermal stabilities of the grains, and the annealed samples were cooled from 753 K to room temperature gradually in the furnace.

2.2. Characterization of the composites

The powder morphologies were examined using scanning electron microscopy (SEM, Quanta 600). The microstructures of the composites were examined using transmission electron microscopy (TEM, Tecnai G2 20). The elastic modulus of the composites was measured by the ultrasonic-resonance method using RFDA-HTVP1750-C (IMCE). The specimens with dimensions of $40 \times 4 \times 1\ mm^3$ were machined with the length parallel to the extruding direction.

Tensile specimens with a gauge length of 5 mm, a width of 1.7 mm and a thickness of 1 mm were machined from the as-extruded composites paralleled to the extruding direction. At least 5 tensile specimens were tested for each composite at a strain rate of $1 \times 10^{-3}\ s^{-1}$ at room temperature on using Instron 5848 tester. Arithmetic average and mean square deviations were respectively used for plotting average value and error bars. For comparison, the tensile test of the Al-5Mg alloy was also conducted under the same conditions.

3. Results

3.1. CNT distributions under different milling rotation rates

The morphology evolutions of the CNT-Al powders with ball-milling time at 300 rpm, 400 rpm and 450 rpm are presented in Fig. 2. Both flattening and coarsening of the powders were observed under different milling durations for these three milling rotation rates. The flattening and coarsening corresponded to the deformation and cold-welding stages of the mill process, respectively [14,15]. At 300 rpm of milling, the flattening of Al powders was slight at 2 h (Fig. 2(a)) and the powders were still coarse flaky powders but not equiaxial powders even after 8 h of milling (Fig. 2(c)), which could be attributed to relatively low energy input. At 400 rpm of milling, the flattening of Al powders was much severe at 2 h (Fig. 2(d)), and powders began to be cold-welded at 6 h (Fig. 2(e)) and finally changed to coarse equiaxial powders at 8 h (Fig. 2(f)). By comparison, the coarsening of Al powders at 450 rpm was even severer. Powders began to coarsen at as early as 4 h milling (Fig. 2(h)) and transferred to coarse powders at as early as 5 h milling (Fig. 2(i)), which was the result of high energy input.

Fig. 3 shows CNT distributions in extruded composites under different milling conditions. CNT bundles could be observed for the composite under 300 rpm milling for 8 h (Fig. 3(a)), and many CNT clusters with a size of about 100 nm were dispersed in the composite under 450 rpm milling for 5 h (Fig. 3(d)). By comparison, CNTs were uniformly dispersed in the composite under 400 rpm milling for 8 h (Fig. 3(c)) but not for 6 h (Fig. 3(b)). In the following parts, the milling conditions for the CNT/Al-5Mg composites were all 400 rpm and 8 h if no special explanation was provided.

3.2. Grain and CNT-Al interface structure

Fig. 4 shows the grain structures of the CNT/Al-5Mg composites. Grain refinement could be observed with the addition of CNTs. The average grain size of the Al-5Mg alloy was about 0.5 μm (Fig. 4(a)). As the CNT concentration increased to 1.5 and 3 vol.%, the average grain size decreased to about 0.3 and 0.2 μm (Fig. 4(b) and (c)), respectively, which is believed to result from the effective pinning effect of CNTs on the recrystallized grains. The grain refinement phenomenon has also been found in other CNT/metal composites

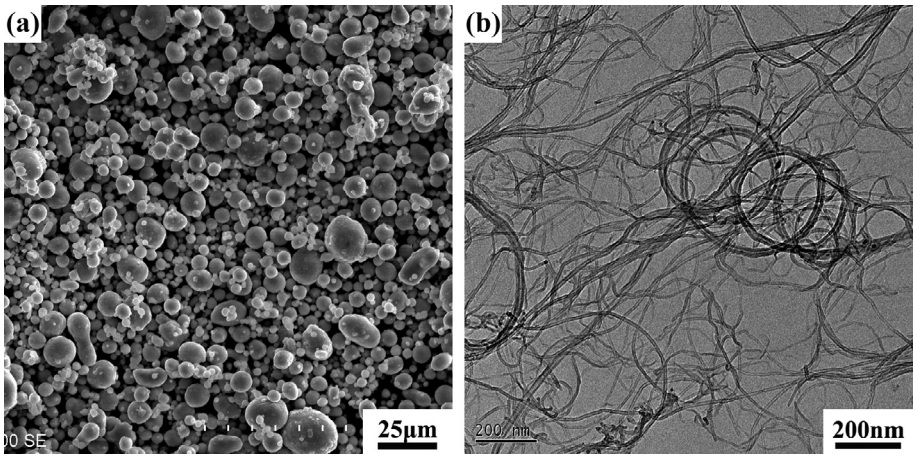

Fig. 1. Morphology of as-received powders: (a) Al-5Mg and (b) CNTs.

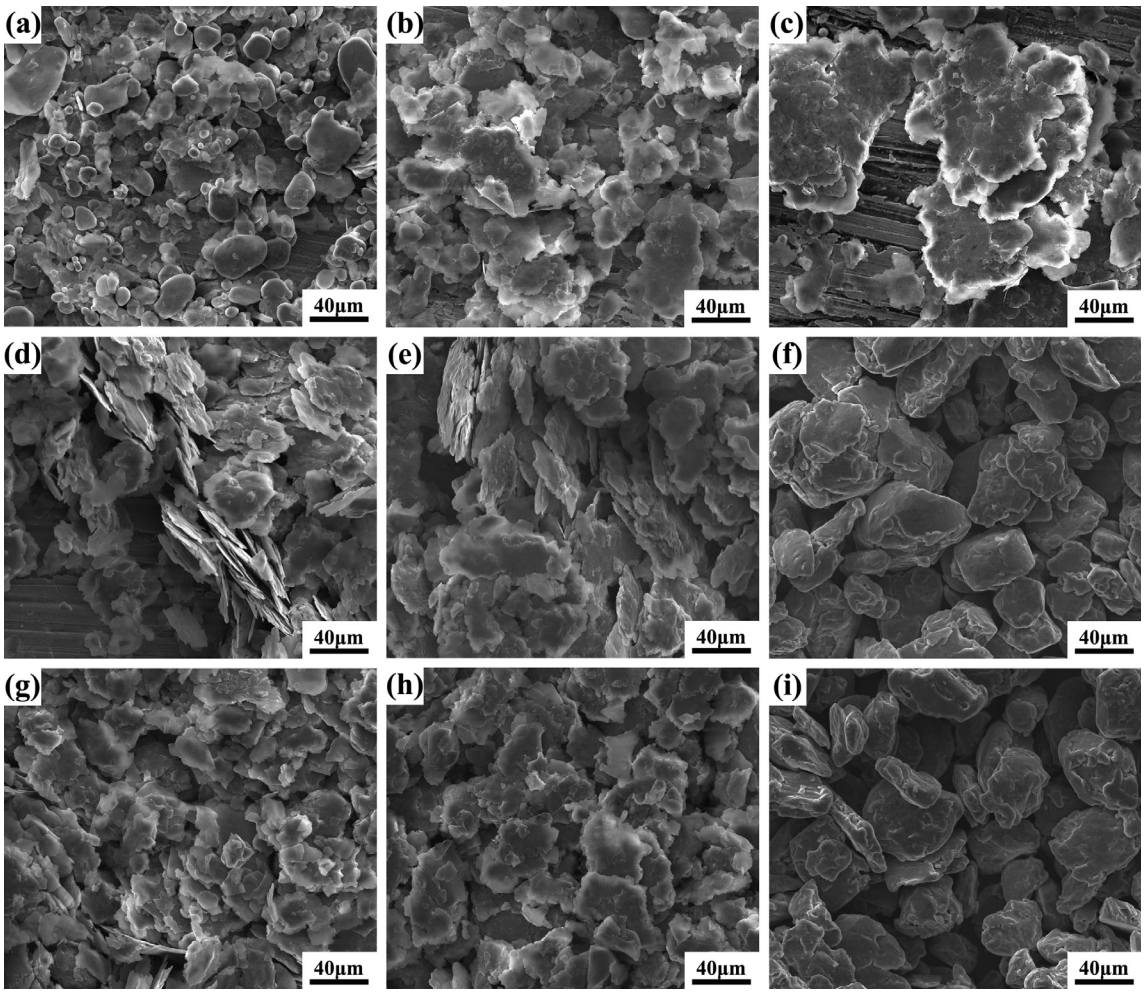

Fig. 2. Morphology of CNT/Al-5Mg powders at (a) 300 rpm, 2 h, (b) 300 rpm, 6 h, (c) 300 rpm, 8 h, and (d) 400 rpm, 2 h, (e) 400 rpm, 6 h, (f) 400 rpm, 8 h, and (g) 450 rpm, 2 h, (h) 450 rpm, 4 h, (i) 450 rpm, 5 h.

[4,5,16], e.g. the average grain sizes of 1.5, 3 and 4.5 vol.% CNT/2009Al composites fabricated by friction stir processing [16] were 3, 0.8 and 0.5 μm, respectively. The grains of the annealed 3 vol.% CNT/Al-5Mg composites are shown in Fig. 5. The grain size of the annealed composites remained relatively stable even at 753 K (Fig. 5(a)–(c)), and this grain thermal stability was also reported in a previous study at 773 K for 3 vol.% CNT/Al-11Zn-2Mg-Cu [17].

Fig. 6(a) shows the fine microstructures of the composites. It was observed that CNTs with a length of ~200 nm were singly dispersed in Al matrix and approximately aligned along the extruding direction. The CNT length became much shorter compared with that of the as-received CNTs, which could be attributed to severe shear effect during milling. Furthermore, a small amount of Al_4C_3 were detected to be close to or attached to CNTs in some local zone. Ci et al. [18] also found that CNT-Al reaction could occur due to the presence of defect sites and open-ends in CNTs, even the fabrication temperature was below the Al melting point.

High resolution TEM images shown in Fig. 6(b) indicated that most of CNT-Al interfaces were bonded well and the CNT structure integrity was well retained. For some CNTs with local structure defects, CNT-Al reaction occurred at the local sites and Al_4C_3 (5–20 nm in size) were observed (Fig. 6(c)). TEM examination in Fig. 6(d) revealed the existence of the dislocations at the CNT interface of the composite and this would be discussed later. Fig. 7 shows the XRD diffraction pattern of 3 vol.% CNT/Al-5Mg composite. Only two peaks of Al_4C_3 with very weak peak intensity could be identified. This indicates that the Al-CNT interface reaction was not severe, which was in accordance with the TEM results shown in Fig. 6.

For the reaction $4Al + 3C = Al_3C_3$, the Gibbs free energy is:

$$\Delta G = -75,211 + 17.4T \quad (1)$$

where T is the temperature.

According to Eq. (1), at temperatures between room temperature and 4322 K, the Gibbs free energy is negative, indicating that the Al_4C_3 formation is a spontaneous reaction. It is well known that the presence of Al_4C_3 would result in degradation of the composites in the atmospheric moisture [19,21]. The Al_4C_3 formation is mainly determined by atom diffusion. As the temperature decreased, the atom diffusion rate was reduced and therefore the Al_4C_3 formation was restrained. More importantly, the solidus temperature for the Al-5Mg alloy is about 850 K, which means that no liquid appeared for the composite hot-pressed at 753 K. Further, the Al_2O_3 membranes between Al and CNTs could also inhibit the CNT-Al reaction. As a result, the CNT-Al reaction could be greatly inhibited and good bonding of CNT-Al could be obtained in this work.

It should be mentioned that the minimal CNT-Al reaction without much damage to CNT structure is desirable for the composites. For example, Stein et al. [22] fabricated CNT/5083Al composites by ball milling-PM route at a much lower hot-consolidation

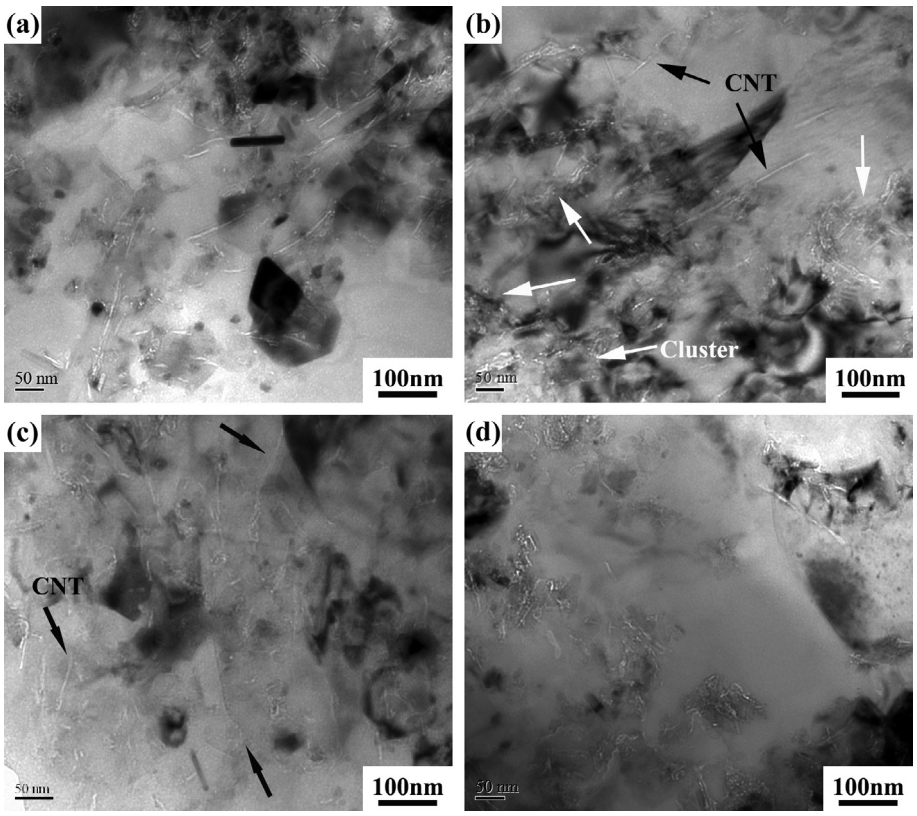

Fig. 3. CNT distributions in CNT/Al-5Mg powders at: (a) 300 rpm, 8 h, (b) 400 rpm, 6 h, (c) 400 rpm, 8 h, (d) 450 rpm, 5 h.

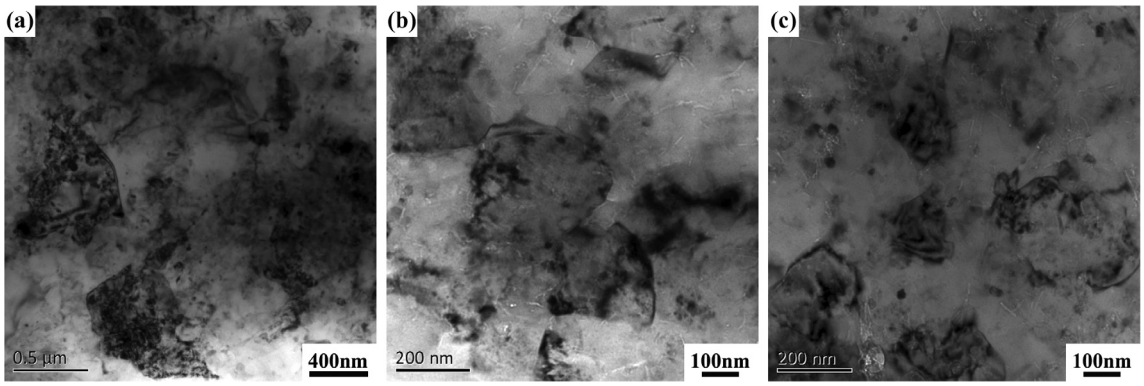

Fig. 4. TEM images showing grains of CNT/Al-5Mg composites with CNT concentrations of (a) 0, (b) 1.5, and (c) 3 vol.%.

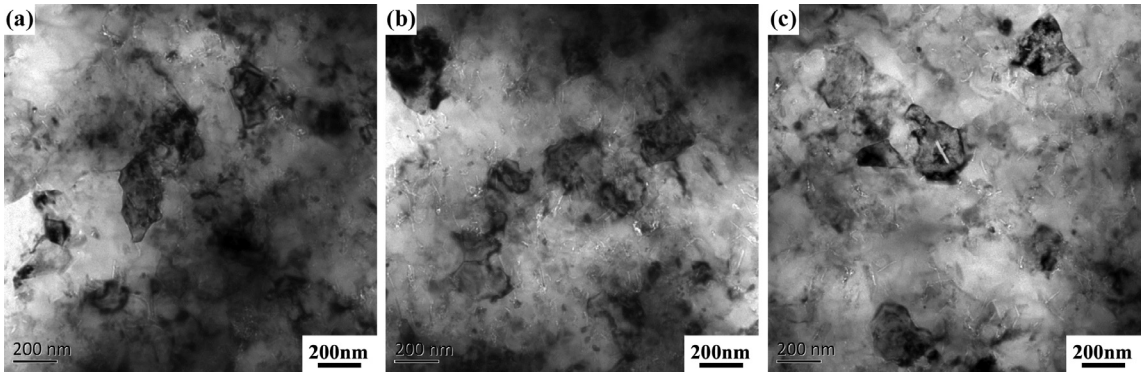

Fig. 5. Grain sizes of 3 vol.% CNT/Al-5Mg composites annealed for (a) 1 h, (b) 2 h, (c) 4 h.

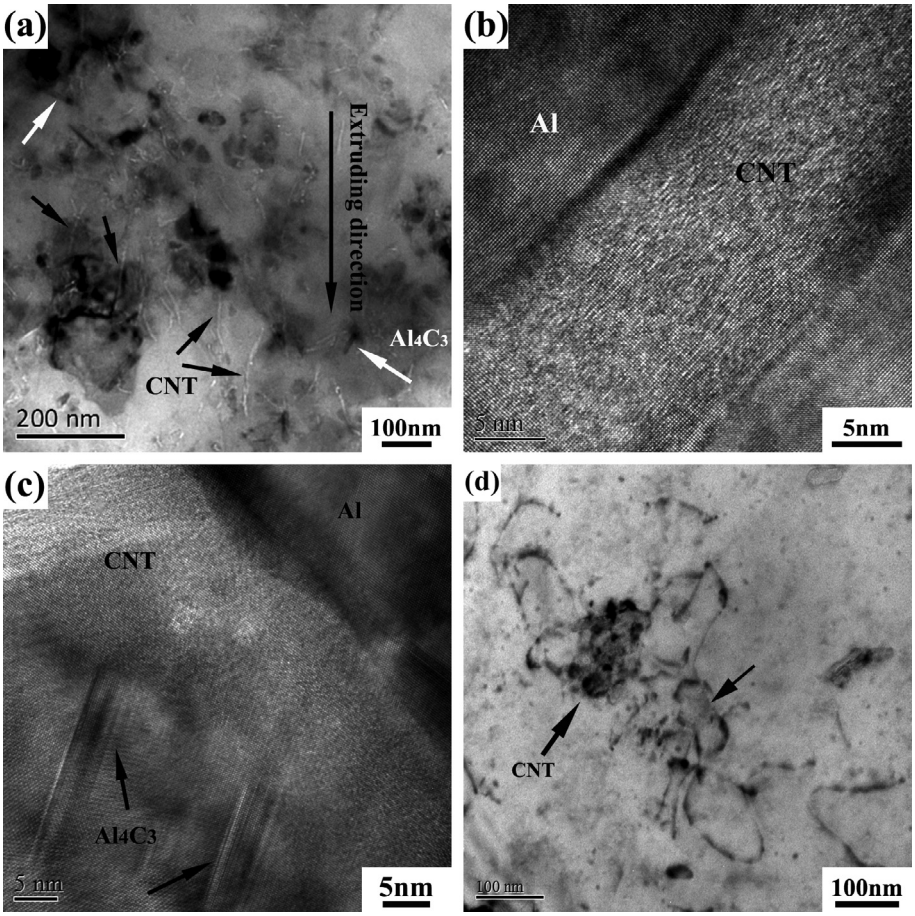

Fig. 6. TEM images showing microstructure in composites: (a) CNT distribution, (b) clean Al-CNT interface, (c) reacted Al-CNT interface and (d) dislocations near to CNTs.

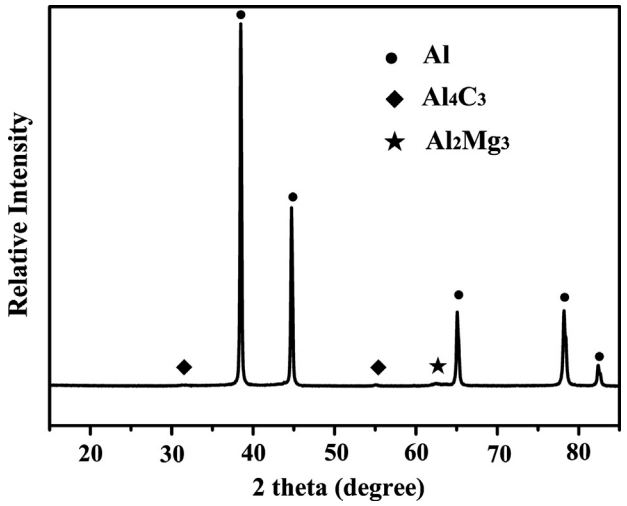

Fig. 7. XRD diffraction pattern of 3 vol.% CNT/Al-5Mg composite.

temperature of 623 K. They found that the strengths of the composites were increased, however, the elongations were much lower and the Young's moduli were not increased compared with that of the matrix alloy. As well-known, CNTs and Al had poor wetting properties, low hot-consolidation temperature of 623 K led to weak interface bonding due to the lack of reaction. As a result, poor elongation and modulus were achieved.

3.3. Tensile properties of the composites

Table 1 shows the tensile properties of the Al-5Mg alloy and CNT/Al-5Mg composites. The yield strength (YS) and the ultimate tensile strength (UTS) of the composites were substantially increased compared with those of the matrix alloy. Increasing the CNT concentration from 1.5 to 3 vol.% led to increase in both YS and UTS. The elastic modulus of the composites was also increased due to the high modulus of CNTs, and the composite with 3 vol.% CNTs reached to 86 GPa, much higher than that for the Al-5Mg alloy (73 GPa).

The typical engineering stress-strain curves of the composites are shown in Fig. 8(a). CNTs led to increased work-hardening and greatly reduced elongation (El). CNT and Al matrix has great different tensile properties, mismatch dislocation might be induced at the interface during tension and the dislocation could hinder the movement of other dislocations, which resulted in increased work-hardening. The reduced El is attributed to the fracture mode of the composite. Composite fracture is directly related to the interfacial failure or reinforcement cracking. Micro-voids tend to form at low strains during tension due to the stress concentration

Table 1
Tensile properties of Al-5Mg and CNT/Al-5Mg composites.

Sample	E (GPa)	YS (MPa)	UTS (MPa)	El. (%)
Al-5Mg alloy	73 ± 1	340 ± 5	410 ± 8	12 ± 2
1.5 vol.% CNT/Al-5Mg	80 ± 1	449 ± 8	506 ± 10	7 ± 1
3 vol.% CNT/Al-5Mg	86 ± 1	554 ± 9	610 ± 9	3 ± 1

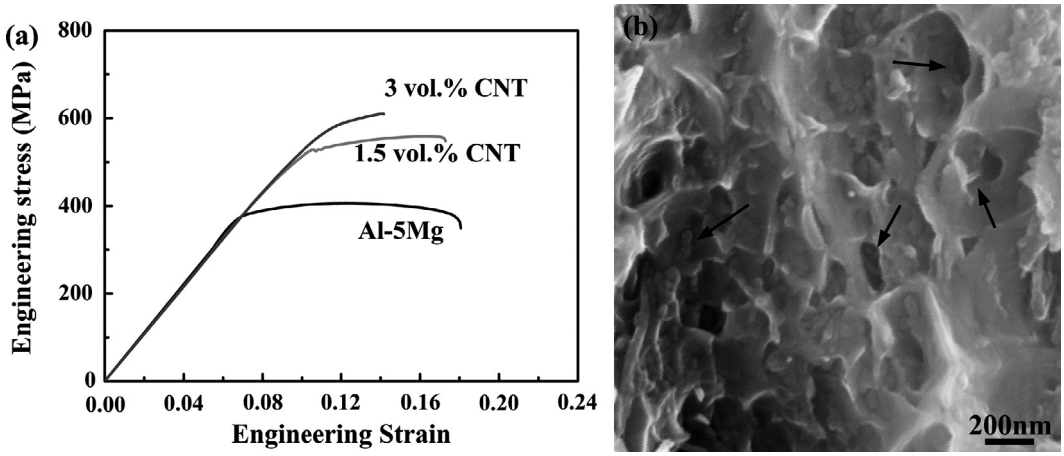

Fig. 8. (a) Engineering strain-stress curves of CNT/Al-5Mg composites and matrix alloy, (b) fractograph of 3 vol.% CNT/Al-5Mg composite.

Table 2
YS of 3 vol.% CNT/Al-5Mg composites after different annealing durations at 753 K.

Annealing duration (h)	0	1	2	4
YS (MPa)	554 ± 9	521 ± 7	523 ± 7	516 ± 8

at the CNT-Al interfaces, resulting in a low level of El. Fractograph of 3 vol.% CNT/Al-5Mg composite is showing in Fig. 8(b). Many CNTs with tips outside were observed at the bottom of the dimples, which also indicated that the micro-voids originated at the zone near CNTs.

The YS of the composite decreased by about 30 MPa after annealing at 753 K for 1 h, and then remained stable for annealing from 2 to 4 h (Table 2). It was reported that CNTs and Al did not severely react at the temperature lower than solidus temperature [18]. It means that CNTs would not suffer severe damage during the annealing treatment whose temperature is much lower than the solidus temperature of about 850 K. The grain size of the annealed composites remained stable at 753 K (Fig. 5). Thus, the YS decrease of the composites with annealing might be attributed to the change in dislocation density during annealing. This would be discussed later.

4. Discussion

4.1. CNT distribution model during milling

According to the milling mechanism, in the deformation stage, the ductile powders were milled into flaky morphology, while large CNT clusters were fractured into small ones and dispersed along the boundaries of flaky powders (Fig. 9(a)). In the cold-welding stage, the flaky powders were cold-welded into laminate structure and the brittle particles were thus introduced into ductile powders. This means that the uniformity of CNT distribution was greatly determined by Al powder deformation and CNT dispersion prior to the cold-welding stage.

According to the powder fraction changing theory during milling proposed by Aikin et al. [23], as the milling duration increases from 0 to t, the fraction of Al powders changes from $f_{Al,0}$ to f_{Al}. The relationship between duration and powder fraction can be expressed as:

$$\frac{f_{Al}}{1-f_{Al}} = \frac{f_{Al,0}}{1-f_{Al,0}} \exp\left(-\frac{at}{\tau}\right) \tag{2}$$

where a is the probability of cold-welding, τ is the time interval between two different ball collisions, which can be expressed as:

$$\tau = \lambda / v \tag{3}$$

where λ is the mean free path of balls during milling and v is the mean velocity of balls before collision.

As the fraction of Al powders decreases to a certain value, cold-welding can be considered to be dominant. The duration $t_{flatten}$ for flattening of Al powders can be calculated as:

$$t_{flatten} \propto \tau = \lambda / v \tag{4}$$

Evolution of CNT cluster sizes are (the derivation detail could be found in Appendix A):

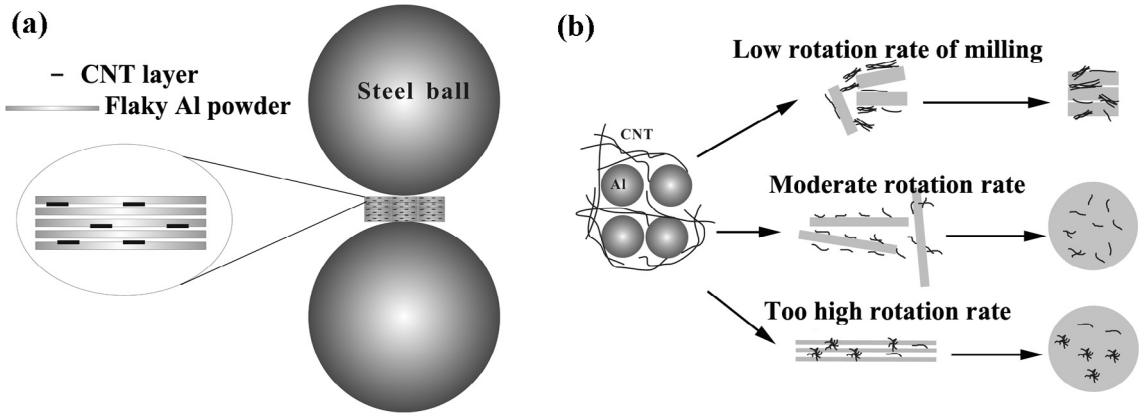

Fig. 9. Schematic of (a) CNT-Al powders captured by balls during milling and (b) CNT distributions during milling at different rotation rates.

$$D^{-3} - D_0^{-3} = \zeta \varepsilon t \tag{5}$$

where ζ is a coefficient, ε is the imposed strain on the CNT/Al powders during milling.

As the cluster size decreases to some small value, CNT clusters can be regarded to disappear. It means that the minimum necessary time for dispersing CNTs should be:

$$t_{CNT-dispersion} \propto \varepsilon^{-1} \tag{6}$$

The ε during milling has a relationship with velocity of balls before collision v according to calculation proposed by Maurice [24,25]:

$$\varepsilon \propto v^{0.4} \tag{7}$$

Eq. (6) can be changed to:

$$t_{CNT-dispersion} \propto v^{-0.4} \tag{8}$$

The ratio of minimum necessary time for dispersing CNTs to flattening time of Al is:

$$t_{CNT-dispersion}/t_{flatten} \propto v^{0.6} \tag{9}$$

From Eq. (9), larger ball velocity corresponding to larger mill rotation rate leads to larger ratio of minimum necessary time for uniformly dispersing CNTs to flattening time of Al powders. That is, dispersing time for CNTs might not be enough at higher milling rotation rate, as cold-welding could be shifted to a much early time.

The relationship between CNT distribution and rotation rate could be indicated in Fig. 9(b). At a lower rotation rate of 300 rpm, CNTs had enough time to disperse as cold-welding was delayed according to Eq. (9), but no enough specific surface areas of Al powders could be provided for CNT distribution. As a result, CNTs could not be singly dispersed (Fig. 3(a)). At a much higher rotation rate of 450 rpm, the time for powder flattening was greatly reduced compared with that for uniformly dispersing CNTs, according to Eq. (9). Although flaky powders with thin thickness could provide larger surface for CNT distribution, cold-welding was severe and appeared at much earlier stage during milling (Fig. 2(h)). Some small-sized CNT clusters were easily cold-welded into Al powders, and as a result, many fine CNT clusters could be observed in the composite (Fig. 3(d)).

For a medium rotation rate of 400 rpm, on one hand, enough deformation of Al powders could be provided for producing flaky Al powders with thinner thickness and larger surface for CNT dispersion (Fig. 2(d)). On the other hand, CNT clusters could be dispersed for longer duration as the cold-welding was not too severe. As a result, CNTs could be singly dispersed in the composites under milling at 400 rpm for 8 h (Fig. 3(c)).

There are about three stages during milling: deformation, cold-welding and balanced stage. During deformation stage, ductile Al powders were flattened into flaky powders with larger specific surface, and CNTs were fractured and then dispersed at the boundaries of flaky Al powders. At the cold-welding stage, flaky Al powders were cold-welded into coarse flaky Al powders and CNTs were fixed at the welded seams. Once CNTs were fixed, they were hard to be further dispersed. Therefore, the minimum necessary time for milling should be chosen at the final stage of cold-welding to ensure enough deformation of Al powders and dispersing of CNTs. That is why no CNT clusters were observed for composites milled at 400 rpm for 8 h (Fig. 3(c)), but some CNT clusters were observed for composites milled at 400 rpm for 6 h (Fig. 3(b)).

4.2. Strengthening mechanism

4.2.1. Orowan strengthening

The motion of the dislocation might be inhibited by CNTs, leading to bending of dislocations between CNTs. It induces a back stress, which will prevent further dislocation migration and result in a strength increase. That is the well-known Orowan strengthening mechanism, which is greatly dependent on the mean free path d_0 of CNTs. For simplified calculation, d_0 could be calculated from:

$$d_0 = d_{equ}\sqrt[3]{\pi(6V_f)^{-1}} \tag{10}$$

where d_0 is the mean free path of CNTs and d_{equ} is the equivalent diameter of CNTs.

The strength increase induced by Orowan mechanism $\Delta\sigma_{OR}$ could be calculated by:

$$\Delta\sigma_{OR} = \frac{2.43Gb}{2\pi(1-\upsilon)^{0.5}d_0}\ln\left(\sqrt{\frac{2}{3}}\frac{d_{equ}}{r_0}\right) \tag{11}$$

where b is Burgers vector, G is Shear modulus of matrix, υ is Poisson ratio, r_0 is the core radius of dislocation. It should be pointed out that only the CNTs distributed in the grains could prevent dislocation migration and result in a strength increase. Actually, ex-situ reinforcements tend to be dispersed at grain boundaries, because incoherent phase interfaces have much higher interface energy. Eq. (11) changed to:

$$\Delta\sigma_{OR} = \frac{2.43Gb}{2\pi(1-\upsilon)^{0.5}d_0}\frac{V_{OR}}{V_f}\ln\left(\sqrt{\frac{2}{3}}\frac{d_{equ}}{r_0}\right) \tag{12}$$

where $\frac{V_{OR}}{V_f}$ is the concentration ratio of CNTs in the grains to the whole CNTs.

Assuming that CNTs were randomly dispersed at the grain boundaries and in the grains, the calculation schematic for $\frac{V_{OR}}{V_f}$ is shown in Fig. 10 with two situations:

For composites with relatively large grain sizes:

$$V_{OR} = \frac{(d-2d_0)^3V_f}{d^3} = V_f\left(1-\frac{2d_0}{d}\right)^3 \quad d > 2d_0 \tag{13}$$

For composites with relatively fine grain sizes:

$$V_{OR} = 0 \quad d \leqslant 2d_0 \tag{14}$$

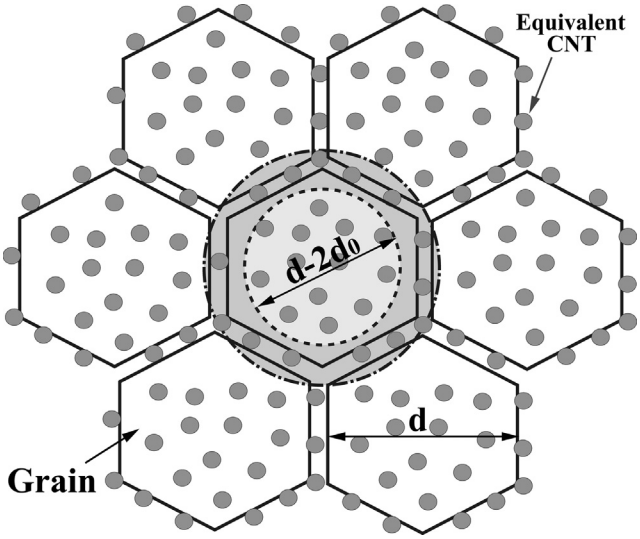

Fig. 10. Schematic of calculation for CNT concentration in the grain.

where d is the average grain size.

In this study, the length and diameter of CNTs were 200 nm and 10 nm, thus the equivalent diameter of CNTs d_{equ} was ~49 nm if CNTs were equivalent to spherical particles. Thus, mean free path of CNTs d_0 were 160 and 111 nm for 1.5 and 3 vol.% CNT/Al-5Mg composites, respectively. The grain sizes of 1.5 and 3 vol.% CNT/Al-5Mg composites were about 300 and 200 nm, respectively, which means that nearly all of CNTs were dispersed at the grain boundaries according to Eq. (14). Thus, Orowan strengthening could be ignored in this study.

4.2.2. Load transfer and grain refinement strengthening

The rule of mixtures cannot be applied to determine the elastic modulus of CNT/Al composites because it is only valid for continuous fiber reinforced composites. However, elastic modulus of short whisker reinforced composites E_c can be estimated using Tsai-Halpin equation [26]:

$$E_c = E_m(1 + \xi\eta V_f)/(1 - \eta V_f) \tag{15}$$

the parameter η being given by the following equation:

$$\eta = (E_p/E_m - 1)/(E_p/E_m + \xi) \tag{16}$$

the parameter ξ being given by the following equation:

$$\xi = 2s + 40V_f^{10} \tag{17}$$

where E_m and E_p are the elastic modulus of the matrix and CNTs, respectively; V_f is the CNT volume fraction in the composite; s is the aspect ratio of CNTs.

In this study, the length and diameter of CNTs were 200 nm and 10 nm, and thus s was about 20. Elastic modulus of the Al matrix introduced in calculations was 73 GPa. The elastic moduli of CNTs were reported to be 0.5–1 TPa [3], and the elastic modulus value of 0.5 and 1 TPa were respectively used for calculation. The measured and predicted elastic moduli of composites are compared in Fig. 11 (a). The elastic moduli estimated from the rule of mixtures are also shown only for the purpose of comparison. The experimental values appear to be well fitted by the results calculated by Tsai-Halpin equation, which reflects good load transfer efficiency of CNTs.

For the short whisker reinforced metal matrix composites, the tensile strength increases due to load transfer [27] and grain refinement mechanisms are strongly related to the reinforcement length and grain size, and can be estimated through the equation given as [28]:

$$\sigma_c = \left(\sigma_0 + kd^{-1/2}\right)[V_f\varphi(s+2)/2 + (1 - V_f)] \tag{18}$$

where σ_c is the YS of the composite; φ is efficient parameter of load transfer, which could be considered as 1 in the condition of good load transfer efficiency; σ_0 is rationalized as a frictional stress to the motion of dislocation glide, and k is the Hall-Petch slope (for annealed Al-Mg alloy, it is about 63 MPa $\mu m^{1/2}$ [29]).

The measured and predicted YS of composites are compared in Fig. 11(b). The YS estimated from the load transfer mechanism is also shown for the purpose of comparison. It is noted that a combination of load transfer and grain refinement mechanisms gives a prediction closer to the experimental value. However, there were still about 10% deviations between the predicted and measured YS values. This means that besides the load transfer and grain refinement, other strengthening mechanisms also contribute to the strength increase.

4.2.3. Mismatch dislocation strengthening

George et al. [30] pointed out that thermal mismatch dislocations would contribute to strengthening of the CNT/metal composites. Thermal mismatch dislocations are induced during cooling after extrusion, because of the large difference in the coefficient of thermal expansion between Al and CNTs. According to previous investigations [31,32], the density of the thermal-mismatch dislocations decreases greatly as the size of the reinforcement decreases to nano-scale. In the present CNT/Al-5Mg composite, CNTs had an average length of 200 nm and a diameter of ~10 nm. Thus, the thermal-mismatch dislocations were not dominant.

Lahiri et al. [33] found that CNTs resulted in extra increase in dislocation density due to non-uniform deformation between CNTs and the matrix. During extrusion, deformation mismatch dislocations were induced at the CNT-Al interface. These dislocations could be relaxed by recrystallization during extrusion. However, the fine and dispersed CNTs in the CNT/Al-5Mg composite inhibited the recrystallization of the matrix. Thus, many dislocations would be retained near CNTs. As shown in Fig. 6(d), many dislocations were observed near CNTs, which might be the extra dislocations due to deformation mismatch between CNTs and Al. The deformation mismatch dislocations induced during extrusion could not be fully eliminated by the recrystallization. As a result, the YS of composites predicted by Eq. (13) were lower than the experimental values. Actually, the YS of the annealed 3 vol.% CNT/Al-5Mg composite was 516 MPa, very close to the predicted value of 510 MPa by Eq. (13). During annealing, the mismatch dislocations could gradually be relaxed as a result of dislocation reaction, and the extra dislocation density could be reduced after annealing. This means that the mismatch dislocations induced by CNTs also contribute to the strength increase of the composites.

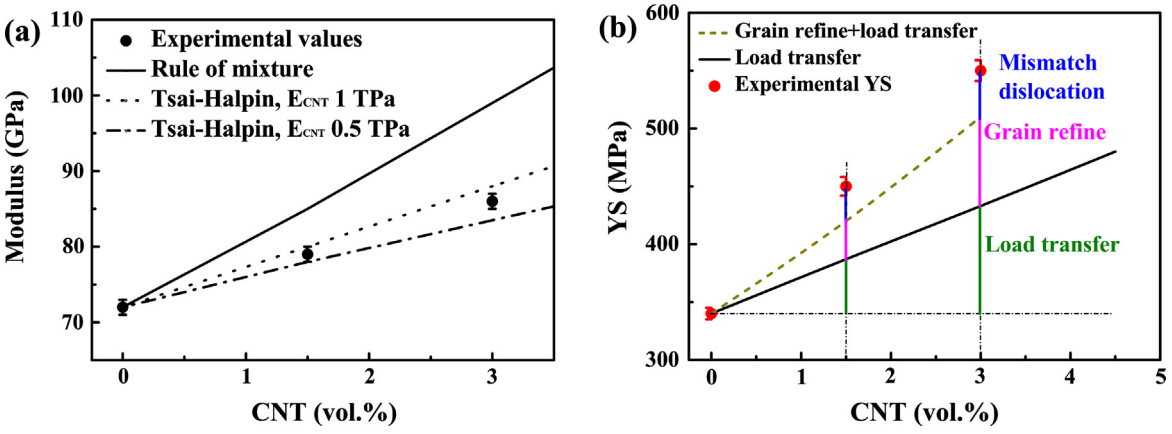

Fig. 11. Comparison between theoretically predicted and experimentally measured (a) elastic modulus and (b) YS for CNT/Al-5Mg composites.

The strengthening contributes due to load transfer, grain refinement and mismatch dislocation could be demonstrated in Fig. 11 (b). The good CNT-Al interface bonding could well transfer load from Al to CNTs with relatively high aspect ratio, which made load transfer the main strengthening mechanism. CNTs introduction also induced severe grain refinement and mismatch dislocations, and they also played important role in strengthening.

5. Conclusions

(1) Milling rotation rate had significant effect on deformation of Al powders, fracture of CNT clusters and cold-welding of composite powders. Both lower rotation rate of 300 rpm and higher rotation rate of 450 rpm were not beneficial to CNT distribution. Medium rotation rate of 400 rpm could provide enough energy for Al powder deformation and avoid too severe cold-welding, which led to single dispersion of CNTs.

(2) A model based on the deformation of Al powders and the ratio of minimum necessary time for dispersing CNTs to flattening time of powders is proposed to evaluate the influence of milling rotation rate on CNT distribution. At high milling rotation rate, flattening time decreases much faster than the minimum necessary time for dispersing CNTs, resulting in that CNT clusters can be cold-welded into Al powders. By comparison, low milling rotation rate leads to longer minimum necessary time for dispersing CNTs and small deformation of Al powders, which is also detrimental to CNT distribution.

(3) The elastic modulus of the CNT/Al-5Mg composites increased as CNT concentration increased, which can be predicted by the Tsai-Halpin equation. The tensile strength of the composites showed a significant increase compared with the matrix alloy, attributing to load transfer, grain refinement and mismatch dislocation mechanisms due to the addition of CNTs.

Acknowledgements

This work was supported by: (a) the National Basic Research Program of China (grant No. 2012CB619600); (b) the CAS-SAFEA International Partnership Program for Creative Research Teams and (c) the National Natural Science Foundation of China (grant No. 51501189).

Appendix A

CNT clusters tend to fracture into small parts during milling. In order to describe the variation in the CNT cluster size, let us assume that the fracture of clusters occurs due to the strain imposed on the CNT/Al powders and that the probability of cluster fracture is dependent on the cluster volume (for simplicity a linearized Weibull model is used). With the above assumptions, the probability of fracture of a cluster p is:

$$p = \mathrm{kD}^3\varepsilon \tag{19}$$

where k is a constant, D is the diameter of CNT clusters, and ε is the imposed strain on CNT/Al powders during milling.

An assumption is made as follows: if a CNT cluster particle by diameter D fractures the two resultant particles are of approximate size $\mathrm{D}/\sqrt[3]{2}$. During an increment of strain $\mathrm{d}\varepsilon$ the change in diameter is $D - D/\sqrt[3]{2}$. During an increment of strain $\mathrm{d}\varepsilon$ the change in the CNT cluster size is $KD^3\mathrm{d}\varepsilon(D - D/\sqrt[3]{2})$. That is,

$$\mathrm{d}D/\mathrm{d}\varepsilon = -kD^3(D - D/\sqrt[3]{2}) \tag{20}$$

and hence, during a processing history, we can write:

$$D^{-3} - D_0^{-3} = 3(1 - 1/\sqrt[3]{2})k\varepsilon \tag{21}$$

where D_0 is the as-received CNT cluster size and D is the CNT cluster size after milling with some duration time. If similar process is repeated for duration of t, the cluster size can be expressed as:

$$D^{-3} - D_0^{-3} = \zeta\varepsilon t \tag{22}$$

where ζ is coefficient.

References

[1] Moya JS, Lopez-Esteban S, Pecharroman C. The challenge of ceramic/metal microcomposites and nanocomposites. Prog Mater Sci 2007;52:1017–90.
[2] Tjong SC. Recent progress in the development and properties of novel metal matrix nanocomposites reinforced with carbon nanotubes and graphene nanosheets. Mater Sci Eng, R 2013;74(10):281–350.
[3] Coleman JN, Khan U, Blau WJ, Gun'ko YK. Small but strong: a review of the mechanical properties of carbon nanotube–polymer composites. Carbon 2006;44(9):1624–52.
[4] Kim KT, Eckert J, Menzel SB, Gemming T, Hong SH. Grain refinement assisted strengthening of carbon nanotube reinforced copper matrix nanocomposites. Appl Phys Lett 2008;92(12):121901–3.
[5] Jeong YJ, Cha SI, Kim KT, Lee KH, Mo CB, Hong SH. Synergistic strengthening effect of ultrafine-grained metals reinforced with carbon nanotubes. Small 2007;3(5):840–4.
[6] Cao L, Li Z, Fan G, Jiang L, Zhang D, Moon WJ, et al. The growth of carbon nanotubes in aluminum powders by the catalytic pyrolysis of polyethylene glycol. Carbon 2012;50(3):1057–62.
[7] Esawi AMK, Morsi K, Sayed A, Taher M, Lanka S. The influence of carbon nanotube (CNT) morphology and diameter on the processing and properties of CNT-reinforced aluminium composites. Composites Part A 2011;42(3):234–43.
[8] Choi HJ, Shin JH, Min BH, Park JS, Bae DH. Reinforcing effects of carbon nanotubes in structural aluminum matrix nanocomposites. J Mater Res 2009;24(28):2610–6.
[9] Peng T, Chang I. Mechanical alloying of multi-walled carbon nanotubes reinforced aluminum composite powder. Powder Technol 2014;266:7–15.
[10] Esawi A, Morsi K. Dispersion of carbon nanotubes (CNTs) in aluminum powder. Composites Part A 2007;38(2):646–50.
[11] Choi HJ, Shin JH, Bae DH. The effect of milling conditions on microstructures and mechanical properties of Al/MWCNT composites. Composites Part A 2012;43(7):1061–72.
[12] Vu-Bac N, Rafiee R, Zhuang X, Lahmer T, Rabczuk T. Uncertainty quantification for multiscale modeling of polymer nanocomposites with correlated parameters. Composites Part A 2014;68:446–64.
[13] Vu-Bac N, Rafiee R, Zhuang X, Lahmer T, Rabczuk T. Stochastic predictions of interfacial characteristic of carbon nanotube polyethylene composites. Composites Part A 2014;59:80–95.
[14] Benjamin J, Volin T. The mechanism of mechanical alloying. Metall Mater Trans B 1974;5:1929–34.
[15] Zhang DL. Processing of advanced materials using high-energy mechanical milling. Prog Mater Sci 2004;49:537–60.
[16] Liu ZY, Xiao BL, Wang WG, Ma ZY. Developing high-performance aluminum matrix composites with directionally aligned carbon nanotubes by combining friction stir processing and subsequent rolling. Carbon 2013;62:35–42.
[17] Lipecka J, Andrzejczuk M, Lewandowska M, Janczak-Rusch J, Kurzydłowski KJ. Evaluation of thermal stability of ultrafine grained aluminium matrix composites reinforced with carbon nanotubes. Compos Sci Technol 2011;71(16):1881–5.
[18] Ci L, Ryu Z, Jin-Phillipp NY, Ruhle M. Investigation of the interfacial reaction between multi-walled carbon nanotubes and aluminum. Acta Mater 2006;54(20):5367–75.
[19] Rodriguez-Reyes M, Pech-Canul MI, Rendon-Angeles JC, Lopez-Cuevas J. Limiting the development of Al_4C_3 to prevent degradation of Al/SiCp composites processed by pressureless infiltration. Compo Sci Technol 2006;66:1056–62.
[20] Pech-Canul MI, Katz RN, Makhlouf MM. Optimum parameters for wetting silicon carbide by aluminum alloys. J Metall Mater Trans A 2000;31(2):565–73.
[21] Pech-Canul MI, Katz RN, Makhlouf MM, Pickard S. The role of silicon in wetting and pressureless infiltration of SiCp preforms by aluminum alloys. J Mater Sci 2000;35(9):2167–73.
[22] Stein J, Lenczowski B, Anglaret E, Frety N. Influence of the concentration and nature of carbon nanotubes on the mechanical properties of AA5083 aluminium alloy matrix composites. Carbon 2014;77:44–52.
[23] Aikin BJM, Courtney TH, Maurice DR. Reaction rates during mechanical alloying. Mater Sci Eng, A 1991;147:229–37.

[24] Maurice D, Courtney TH. Modeling of mechanical alloying: Part III. Applications of computational programs. Metall Mater Trans A 1995;26:2437–4.
[25] Maurice D, Courtney TH. Modeling of mechanical alloying: Part II. Development of computational modeling programs. Metall Mater Trans A 1995;26:2431–5.
[26] Angers R, Krishnadev MR, Tremblay R, Corriveau JF, Dube D. Characterization of SiCp/2024 aluminum alloy composites prepared by mechanical processing in a low energy ball mill. Mater Sci Eng, A 1999;262(1–2):9–15.
[27] Bakshi SR, Agarwal A. An analysis of the factors affecting strengthening in carbon nanotube reinforced aluminum composites. Carbon 2011;49 (2):533–44.
[28] Liu ZY, Xiao BL, Wang WG, Ma ZY. Singly dispersed carbon nanotube/ aluminum composites fabricated by powder metallurgy combined with friction stir processing. Carbon 2012;50(5):1843–52.
[29] Chino Y, Mabuchi M, Iwasaki H, Yamamoto A, Tsubakino H. Tensile properties and blow forming of 5083 aluminum alloy recycled by solid-state recycling. Mater Trans 2004;45:2509–15.
[30] George R, Kashyap KT, Rahul R, Yamdagni S. Strengthening in carbon nanotube/aluminium (CNT/Al) composites. Scripta Mater 2005;53 (10):1159–63.
[31] Lee J, Earmme Y, Aaronson H, Russell K. Plastic relaxation of the transformation strain energy of a misfitting spherical precipitate: ideal plastic behavior. Metall Trans A 1980;11:1837–47.
[32] Kim C, Lee J, Plichta M. Plastic relaxation of thermoelastic stress in aluminum/ ceramic composites. Metall Trans A 1990;21:673–82.
[33] Lahiri D, Bakshi SR, Keshri AK, Liu Y, Agarwal A. Dual strengthening mechanisms induced by carbon nanotubes in roll bonded aluminum composites. Mater Sci Eng, A 2009;523(1–2):263–70.